A cell type-specific multiomics uncovers a guard cell-specific RAF15-SnRK2.6/OST1 kinase cascade

Hongliang Wang[1,6], Yubei Wang[1,2,6], Rongxia Li[1,2], Weiwei Ren[3], Tian Sang[1,2], Bing Zhao[4], Xiao Wang[4], Xuebin Zhang[4], Shaojun Dai[3], Chuan-Chih Hsu[5], Chun-Peng Song[4], Pengcheng Wang[1,4]

[1]Shanghai Center for Plant Stress Biology, CAS Center for Excellence in Molecular Plant Sciences, Chinese Academy of Sciences, Shanghai 200032, China

[2]University of Chinese Academy of Sciences, Beijing 100049, China

[3]Development Center of Plant Germplasm Resources, College of Life Sciences, Shanghai Normal University, Shanghai 200234, China

[4]State Key Laboratory of Crop Stress Adaptation and Improvement, Henan University, Kaifeng 475004, China

[5]Institute of Plant and Microbial Biology, Academia Sinica, Nangang, Taipei 11529

[6]These authors contributed equally: Hongliang Wang, Yubei Wang.

Correspondence and requests for materials should be addressed to: Chun-Peng Song (songcp@henu.edu.cn), Pengcheng Wang (pcwang@cemps.ac.cn)

SUMMARY

Multicellular organisms such as plants contain different cell types with specialized functions. Analyzing the characteristics of each cell type reveals specific cell functions and enhances understanding of organization and function at the organismal level. Here we report a highly-sensitive and efficient cell type-specific multiomics pipeline, combining simplified flow cytometry-based cell sorting for fluorescent protoplasts and optimized nanoscale proteomics and metabolomics methods, which allow in-depth analysis of the proteomes and metabolomes of a particular cell type. Using this method, we quantitatively compared the proteomes and metabolomes of guard cells and mesophyll cells and revealed that the enrichment of signal transduction-related proteins enables guard cells to respond rapidly to various environmental stimuli. We uncovered a guard cell-specific kinase cascade whereby RAF15 and OST1 mediate ABA-induced stomatal closure. This pipeline can be applied to various cell types in plant or non-plant systems to learn how cells function in highly organized multicellular organisms.

INTRODUCTION

Multicellular organisms such as plants contain different cell types with specialized structures and functions. Dissecting the specific structural and functional information in each cell type is essential to understanding how a particular cell type works and how different cells integrate into a complex organism. Recently, the breakthrough of nucleic-acid-amplification-based DNA and RNA sequencing technologies allowed us to mine the transcriptional heterogeneity in different plant tissues [1-3]. Generally, current single-cell transcriptome techniques use high-throughput and limited depth sequencing of thousands of cells, which enables rapid identification of rare and novel cell types, simultaneous characterization of multiple different cell types and states, and identification of unique marker genes in each cluster/cell type [1]. After understanding the transcriptional heterogeneity of cells, it is necessary to perform in-depth analyses of the proteome, including post-translational modifications (PTMs), and metabolome to understand the specialized structure, function, signal transduction, and metabolism in a particular type/cluster of cells.

However, because proteins cannot be amplified *in vitro* like DNA/mRNA, even cutting-edge mass spectrometry can only identify about 1,000 proteins in a single mammalian cell [4,5]. Comprehensively analyzing the proteome in a single cell is still challenging [6]. Alternatively, enriching for a particular type of plant cell is a realizable approach for in-depth proteomics [7]. However, until now, such single-cell-type proteomics was mainly performed in limited cell types that can easily be isolated, including pollen [8-11], guard cell (GC)[12-14], and mesophyll cell (MC). GC is a specialized epidermal cell that plays an important role in gaseous exchange in and out of plant leaves by regulating the opening and closing of the

stomas. Using GC protoplasts (GCP) isolated by enzyme digestion and centrifugation, several groups performed pioneering single-cell-type proteomic studies in Arabidopsis, *Brassica napus*, and maize, and discovered unique proteins, signal transduction pathways, or metabolism that determine the particular function and development of GC [12-15]. Using fluorescence-activated cell sorting (FACS) and GeLC-MS/MS (in-gel tryptic digestion followed by liquid chromatography-tandem mass spectrometry), proteomic analyses identified nearly 2,000 proteins from six different cell types in the Arabidopsis root tips [16]. A similar study compared the proteomes in epidermal and inner cell lines in Arabidopsis root [17]. However, current methods are applicable to limited cell types and require millions of cells, and the efficiency of cell acquirement and the sensitivity of proteomics needs to be improved.

Here, we used a FACS method to enrich for fluorescent protoplasts. Combining with an optimized nanoscale label-free MS analysis method, we set up a cell type-specific pipeline applicable to proteomics and metabolomics studies of GC and MC, as well as root epidermal cells in Arabidopsis and rice. This pipeline allowed us to identify more than 4,500 proteins and 1,600 metabolites in guard cell protoplasts (GCP) and mesophyll cell protoplasts (MCP), using standard commercial mass-spectrometry machines. Quantitative comparison of GCP and MCP revealed the enrichment of signaling components in GC that may enable GC to respond to various environmental stimuli quickly. We uncovered a unique GC-specific RAF15-SnRK2.6 kinase cascade based on these data, which has a crucial role in ABA-induced stomatal closure. This pipeline can be applied to various cell types in plant or non-plant systems to learn how cells work in highly organized multicellular organisms.

RESULTS

A cell-sorting-based proteomics pipeline for limited plant samples

We set up a FACS method to enrich for fluorescent protoplasts (Figure 1A). We used the *pGC1::GFP* transgenic plants [18], which carry GC-specific expressed GFP, as a model system to test our pipeline. The *pGC1::GFP* leaves were digested into protoplasts, and after removal of tissue fragments by filtration, the protoplasts were subjected to FACS (Figures 1B and 1C). This simplified cell sorting procedure works well to isolate hundreds to millions of GCP from Arabidopsis leaves. We typically isolated up to 10,000 fluorescent GCP from 0.2 g leaf tissue (about 4-6 mature leaves from 3-week-old seedlings). We also optimized a nanoscale protein extraction and digestion procedure (Figure 1A). The enriched fluorescent GCP were lysed in sodium lauroyl sarcosinate (SLS)-sodium deoxycholate (SDC) buffer and directly subjected to trypsin digestion in a single microcentrifuge tube to avoid protein loss in precipitation and transferring (Figure 1A). After one-step desalting on C18 Stage-Tip, the peptides were subjected to LC-MS/MS analysis (Figure 1A). Compared to the guanidine chloride (Gdn-Cl) method optimized for medium-scale plant tissue extract [19,20], the simplified SLS-SDC method allowed us to identify more peptides/proteins, especially for hundreds to thousands of protoplasts. For example, we identified 2,827 peptides, representing 1,012 proteins, from about 500 GCP with the SLS-SDC method, which is nearly two-fold more than with the Gdn-Cl method (Figures 1D, 1E and S1, Dataset S1). The Gdn-Cl method acquired more peptides/proteins from 5,000, and 10,000 protoplasts (Figures 1D and S1), probably because precipitation and resuspension remove metabolites and improve the subsequent enzyme digestion and MS detection. Therefore, our pipeline is suitable for proteomics analysis in

samples with limited material.

The proteomics pipeline can be applied to different cell types

To test if this pipeline is applicable to other types of fluorescent cells, we enriched for protoplasts of root cells in *DR5 rev::GFP* transgenic Arabidopsis (Figures 2A and 2B), a marker line for auxin response [21]. We obtained an average of 6,871 peptides, representing 1,950 proteins, from approximately 1,000 fluorescent protoplasts of *DR5 rev::GFP* (Figure 2C and Dataset S2). GO analysis revealed that proteins involved in root development, auxin transport, translation, response to cold, oxidative stress, and embryo development are enriched in *DR5 rev::GFP* fluorescent protoplasts (Figure S2A and Dataset S2).

A recent single-cell transcriptome study in rice revealed that *pOs01g0248900::VENUS-N7* is strongly expressed in atrichoblasts in rice root tips [22]. We obtained 8,149 peptides, representing 2,232 proteins, from approximately 1,000 fluorescent protoplasts of *pOs01g0248900::VENUS-N7* (Figures 2D-F, Dataset S3). Consistent with the finding that some atrichoblast-enriched genes are involved in cell wall biosynthesis [22], we found server GO terms like Go:0071669 (plant-type cell wall organization or biogenesis) and GO:0071554 (cell wall organization or biogenesis) in the proteins identified in the fluorescent protoplasts of *pOs01g0248900::VENUS-N7* (Dataset S3). Other enriched GO terms included oxoacid and cellular ketone metabolic processes, transport, and glycolysis (Figure S2B and Dataset S3). Therefore, our pipeline is useful for studying a variety of plant cell types.

In-depth proteomics analysis of GCP and MCP

Encouraged by this result, we further performed label-free quantitative proteomics from 1 μg total protein extract from GCP (about 30,000 cells) and MCP (about 15,000 cells) to acquire in-depth proteomic profiles of GCP and MCP. We identified a total of 27,511 peptides, representing 4,622 proteins, in GCP, and 25,235 peptides, representing 4,237 proteins, in MCP (Figure 3A, Dataset S4 and S5). Among these proteins, 526 proteins were identified at least once in the three biological replicates of GCP, but not in any sample of the MCP, and 141 proteins were only detected in MCP (Figure 3A, Dataset S4 and S5). We also performed a quantitative comparison of the GCP and MCP proteomes (Dataset S6-8). As shown in Figures 3B and 3C, 2,483 proteins showed enrichment in GCP (FC > 2, $p < 0.05$) (Dataset S7). Some proteins involved in stomatal development/function were present in the list of GCP enriched proteins (Figures 3D-F). FAMA and Inducer of CBF Expression 1 (ICE1)/ SCREAM (SCRM) govern GC mother division and promote GC differentiation [23]. FAMA, ICE1/SCRM, and their interacting protein, the Third Largest Subunit of Nuclear DNA-dependent Pol II (NRPB3), were present in the list of GCP enriched proteins ($p < 0.05$) [24]. After forming GC, STOMATAL CARPENTER 1 (SCAP1) is required to develop functional stomata [25]. MYB DOMAIN PROTEIN 60 (MYB60) involved in the stomatal movement is a known target of SCAP1 [25]. Both SCAP1 and MYB60 were only present in GCP, not in MCP, in our study. Besides these proteins for stomatal development, we also noticed that known regulators of GC intensity, like MUS, SCD1, and PHYB, were enriched in GC (Figure 3E). Many key components of stomatal movement regulation in response to blue light (BL), high CO_2, and abscisic acid (ABA) were also enriched in GCP (Figure 3F). For example, BETA CARBONIC ANHYDRASE 4 (BCA4) [26], HIGH LEAF

TEMPERATURE 1 (HT1) [27], and CONVERGENCE OF BLUE LIGHT AND CO_2 1 (CBC1)/CBC2 [28], mediating CO_2-induced stomatal movement, and blue light receptors CRYPTOCHROME 2 (CRY2) and PHOT2 [29], the PHOT2 substrate BLUE LIGHT SIGNALING1 (BLUS1) [30] and BLUE LIGHT-DEPENDENT H^+-ATPase PHOSPHORYLATION (BHP) [31], were present in the list of GCP enriched proteins. A recent study suggested that glucose, not malate, is the major starch-derived metabolite in GC for rapid stomatal opening [32]. The b-AMYLASE1 (BAM1) [32], a glucan hydrolase, and ATP-BINDING CASSETTE B14 (ABCB14) [33], the malate transporter, were enriched in GCP. Consistently, the enriched KEGG pathway and enriched GO terms in the GCP were mainly related to transport, RNA degradation, and responses to ABA, cold, and osmotic stress (Figures 3G, S3, and Dataset S9).

There were 664 proteins only present or enriched (FC > 2, $p < 0.05$) in MCP (Figures 3B, 3C, and Dataset S8). Notably, 546 out of these 664 proteins are known to be components of chloroplast (GO term 0009507). Other enriched GO terms of MCP enriched proteins included photosynthesis, photorespiration, pigment, chlorophyll metabolic process, electron transport chain, and response to radiation and light stimulus. These data supported the dominant role of MC in photosynthesis (Dataset S9).

Metabolomics analysis of GCP and MCP

To determine the metabolite differences between GCP and MCP, we also performed untargeted metabolomics using approximately 100,000 GCP or MCP and detected 1,678 metabolites (Dataset S10). Principal component analysis indicated a clear separation of the

metabolomes in the two different cell types (Figure 4A). We found 260 metabolites significantly ($\log_2$ ratio > 0.26, $p < 0.05$, unpaired two-tail *t*-test) enriched in GCP compared to MCP, and 530 metabolites enriched in MCP compared to GCP (Figures 4B and 4C, Dataset S10). Pathway enrichment analysis of the differentially accumulated metabolites indicated an over-representation of metabolites derived from flavone and flavonol biosynthesis (Figure 4D, Dataset S10).

We also performed an integrative analysis combining the proteomics and metabolomics data to reveal the GC-specific metabolic pathway. Several intermediates in flavonoid/phenylpropanoid metabolic pathways, like Kaempferol-3-glucoside-7-O-rhamnoside, Kaempferol, Rutin, and Afzelin, were highly enriched in the GCP ($p < 0.05$, unpaired two-tailed *t*-test) (Figure S4A). Consistently, the enzymes catalyzing flavonoid/phenylpropanoid biosynthesis, like Flavonol Synthase 1 (FLS1), Flavanone 3-hydroxylase (F3H), Transparent Testa 5 (TT5), and Chalcone Isomerase Like (CHIL), were highly accumulated in GCP (Figure 4E and S4B). Previous studies suggested a crucial role of flavonoids in scavenging reactive oxygen species (ROS) in GC [34-36]. The enrichments of these enzymes and metabolites suggest their potential roles in regulating flavonoid metabolism and ROS homeostasis in the GC.

The quick opening and closing of stomata largely depend on the structure of the cell walls [37]. In *gpat4/gpat8*, a mutant lacking two glycerol-3-phosphate acyltransferases (GPAT) required for cutin biosynthesis, the cuticular ledges between GC are defect [38]. Our data showed that several enzymes in cutin biosynthesis, including GPAT4, GPAT8, and a short-chain dehydrogenase ECERIFERUM 3 (CER3), are highly accumulated in GCP

(Dataset S7). Supporting this notion, some enzymes and metabolites in the fatty acid biosynthesis and elongation pathway were highly accumulated in GCP (Figure 4D and S4B).

GC-enriched RAF15 mediates OST1 activation and stomatal closure

We then systemically surveyed the presence of known ABA signaling components in GCP and MCP. Dozens of known ABA signaling components showed a GC-enriched pattern, and only very few components had a higher abundance in MCP than in GCP (Figure 5A). For example, the ABA receptors PYR1, PYL1, and PYL2 showed 65.8-, 5.6-, and 446-fold enrichment, respectively, in GCP, while PYL4 was only detected in the GCP, not in the MCP (Figure 5B). SnRK2.6/OST1 (a master regulator of stomatal movement) and ABI2 showed 34.0- and 4.9-fold enrichment, respectively, in GCP (Figure 5B). By contrast, ABI1 showed an accumulation in MCP (Figure 5B). To our surprise, the B2 and B3 subgroup RAF kinases, known to phosphorylate and activate SnRK2.2, SnRK2.3, and SnRK2.6/OST1 in response to ABA [39-41], were not detected/enriched in our proteomics result (Figure 5B). This suggested that kinases other than B2 and B3 RAFs may contribute to ABA-induced SnRK2.6/OST1 activation and stomata closure.

Our GCP proteomics identified RAF15 (AT3G58640) in the B1 subgroup, BHP/RAF27 in the C1 subgroup, HT1/RAF19 in the C5 subgroup, RAF28 in the C6 subgroup, and CBC1/RAF38, CBC2/RAF33, and AtMRK1/RAF48 in the C7 group (Figure 5C). Consistently, most of these genes showed higher expression in GCP than in MCP (Figures S5A and 5B). Using a transient expression assay system in MCP of *OK*^{100}*-nonu*, which lacks most members of the B2 and B3 RAFs involved in ABA signaling, and has very low

expression of SnRK2.6/OST1, we evaluated the function of these B1 and C subgroup RAFs in ABA signaling [41]. Co-transfection of SnRK2.6/OST1 alone did not rescue the expression of ABA-induced *RD29B-LUC* in MCP of *OK*^{100}*-nonu* (Figure 5D). However, co-transfection of RAF15, BHP/RAF27, HT1/RAF19, CBC1/RAF38, or MRK1/RAF48, but not RAF28 or CBC2/RAF33, rescued the expression of ABA-induced *RD29B-LUC* in MCP of *OK*^{100}*-nonu* (Figure 5D). An *in vitro* kinase assay showed that full-length HT1/RAF19 or RAF15, out of the five tested RAFs, could directly phosphorylate SnRK2.6^{KR}, a kinase "dead" form of SnRK2.6/OST1 (Figure 5E). Two serine residues in the activation loop of SnRK2.6/OST1, Ser171 and Ser175, are known to be phosphorylated by B2 and B3 RAFs, and their phosphorylation is essential for SnRK2.6/OST1 activation [22,42,43]. Site-direct mutagenesis of Ser171 and Ser175 showed that RAF15 mainly phosphorylates the Ser175 in SnRK2.6 and the Ser175Ala mutation abolished the phosphorylation of SnRK2.6/OST1 by RAF15 (Figure 5F). Neither Ser171 nor Ser175 was the HT1/RAF19 phosphosite in SnRK2.6/OST1 (Figure S5C).

We then tested if RAF15 could reactivate the dephosphorylated inactive form SnRK2.6 (de-SnRK2.6). We used an adenosine triphosphate (ATP) analog-based *in vitro* kinase assay system, which can distinguish the trans- and autophosphorylation of SnRK2.6, to monitor the activity of SnRK2.6/OST1 [41]. A Met94Gly (M94G) mutation in SnRK2.6/OST1 enlarges its ATP binding pocket, which can use the ATP analog N^6-Benzyl-ATPγS to thiophosphorylate itself or its substrate [41]. By this method, thiophosphorylation by activated SnRK2.6^{M94G} can be detected with an anti-thiophosphate ester antibody that only recognizes the thiophosphorylation. As shown in Figure 5G, pre-dephosphorylated SnRK2.6^{M94G}

(de-SnRK2.6^{M94G}) had no auto-thiophosphorylation activity (lanes 2-6). Application of the recombinant kinase domain of RAF15 (RAF15-KD) quickly induced the auto-thiophosphorylation of SnRK2.6^{M94G} in a time-dependent manner (lanes 7-10), suggesting that RAF15-mediated phosphorylation is sufficient to reactivate SnRK2.6^{M94G} *in vitro*, in the context of the auto-thiophosphorylation activity of SnRK2.6^{M94G}. We then examined SnRK2.6^{M94G} activity by detecting the thiophosphorylation of ABA□responsive element□binding factor 2 (ABF2), a well-studied SnRK2 substrate. Adding RAF15-KD initiated the thiophosphorylation of SnRK2.6^{M94G} and ABF2 (Figure 5H, lanes 4 and 5). Thus, transphosphorylation by RAF15-KD is sufficient to reactivate the dephosphorylated SnRK2.6/OST1. Unlike RAF15-KD, HT1/RAF19-KD did not reactivate the dephosphorylated inactive de-SnRK2.6 in the *in vitro* activation system (Figure 5I, lane 3 and 4).

We also tested the ABA-induced stomatal closure in *raf15-1* and *raf15-2*, two T-DNA mutant lines of *RAF15* (Figure S5D). Both *raf15-1* and *raf15-2* showed a significantly impaired stomatal closure in response to ABA, compared to wild type (unpaired two-tailed *t*-test, $p < 0.001$) (Figure 5J). RAF13 in the B1 subgroup also phosphorylated Ser171 and reactivated SnRK2.6^{KR} *in vitro* (Figures 5I, lane 5 and 6 and S5E). Another B1 RAF, RAF14, had weak kinase activity and did not phosphorylate SnRK2.6^{KR} *in vitro* (Figure S5F). However, the abundance of *RAF13* and *RAF14* mRNA in GC was much less than that of *RAF15* mRNA (Figure S5A), and RAF13 and RAF14 protein was not detected in our GC proteomics (Dataset S4). We also noticed that all three members of the B1 RAF subgroup failed to phosphorylate SnRK2.4^{KR}, one of the ABA-independent SnRK2s (Figure S5G).

Thus, GC-enriched RAF15 may have a unique role in stomatal closure through specifically mediating ABA-induced SnRK2.6/OST1 activation (Figure 5K).

DISCUSSION

Here, by optimizing the sample preparation and detection procedures, we developed a cell-sorting-based nanoscale pipeline that allows in-depth profiling of the proteome and metabolome of various cell types in plants. We can routinely isolate up to 10,000 protoplasts from a few leaves of Arabidopsis seedlings and identify more than 4,500 unique proteins and 1,600 metabolites in GCP. Compared to pioneering studies that identified approximately 2,000 proteins from 1,000,000 root cell protoplasts [16], and 2,000 proteins and 300 metabolites from 3×10^8 GCP [13,44], our method showed a significantly improved sensitivity and efficiency. Importantly, this pipeline is also applicable to root cells in both Arabidopsis and rice, suggesting the potential of this pipeline in multiomics analysis in different cells from different plant species and even non-plant systems. Combined with the single-cell-transcriptomics that identify unique marker genes for each cell group, we may generate fluorescent transgenic lines and perform cell-specific multiomics in each cell type in a tissue or even organism. In the future, this pipeline may also be applied to the sorting and enrichment of different organelles for spatial proteomics to understand the localization and dynamics of proteins in cells [45]. Such enriched cells or organelles could also be used for PTM proteomics to further reveal functional regulation at the proteome level.

As a FACS method, the protoplast isolation method for each cell type needs to be optimized. A few hours' enzymatic digestion with cellulase/macrozyme and high-concentration mannitol may affect the stability or modification of some proteins, which

limits the application of this pipeline in stimulus-responsive proteomics analysis. It is also limited to species than can be transformed. We noticed that some RAFs, e.g., RAF6, that are highly expressed in GC (Figure S5A) were not identified in our GC proteomics, and this might be due to degradation in protoplast/sample preparation. In addition, we failed to obtain enough quiescent center (QC) cells from *WOX5::ERGFP* transgenic plants, which might be due to the limitation of cytometry to isolate a cell type with such low abundance. In the future, new methods like magnetic-activated cell sorting may be helpful to isolate and perform multiomics analysis in such cell types.

The in-depth analysis of proteome and metabolome in GC allows us for the first time to uncover the molecular basis that determines the highly specialized structure and function of GC. SnRK2.6/OST1 is the master regulator in stomatal movement, and dysfunction of OST1 in *ost1* results in an open stomata phenotype even upon drought conditions or pathogen attacks [46,47]. Under unstressed conditions, OST1 is dephosphorylated and inhibited by the A Clade PP2C phosphatases [48]. Upon stress conditions, ABA binds to ABA receptor PYR1/PYL/RCAR proteins, and the ABA/receptor complex inhibits PP2Cs [49-52]. Recombinant SnRK2.6 was considered to be auto-reactivated after being released from PP2C-mediated inhibition [42]. However, recent studies suggested that B2 and B3 subgroup RAF-mediated transphosphorylation is essential for the reactivation of ABA-dependent SnRK2.2, SnRK2.3, and SnRK2.6/OST1 [39-41,43,53]. The high-order mutant of B2 and B3 RAFs, *OK*^{100}*-nonu*, shows an ABA-hyposensitive phenotype in germination and seedling growth, resembling the phenotype of *snrk2.2/2.3/2.6* triple and *pyl112458* high-order mutants [41]. However, although much insensitive to ABA than the wild type, the stomata of

OK[100]*-nonu*, which are still partially closed upon application of ABA, are not identical to those of *snrk2.2/2.3/2.6* triple and *pyl112458* high-order mutants [41]. Here we showed that the GC-enriched B1 subgroup RAF15 also phosphorylates SnRK2.6/OST1 and mediates ABA signaling in GC. Consistently, the *raf15* single mutant already shows impaired stomatal closure in response to ABA. A very recent study suggested that RAF6, a member of the B3 RAF subgroup, has a dominant role in the rapid vapor pressure difference of GC [54]. Both *RAF6* and *RAF15* are highly expressed in GCP, compared to MCP (Figure S5A). Thus, the twenty-two B subgroup RAFs and ten SnRK2s may form complex kinase networks, and different cell types may have unique RAF-SnRK2 cascades. The cell-type specialized signaling pathways may ensure that different cells, depending on developmental stage, nutrition status, or microenvironment, respond to similar environmental clues differentially and precisely.

Besides providing clues for discovering the GC-specific RAF15-SnRK2.6/OST1 kinase cascade, our multiomics data also suggest the molecular basis for some long-standing questions in GC structure and function. For example, we found that enzymes in flavone metabolism are highly enriched in GC. Consistently, intermediates in the flavone biosynthesis pathway are also accumulated in GC, which may ensure the maintenance of ROS homeostasis in GC. Our in-depth proteomics and metabolomics data of GC could be a valuable resource for future study of the structure, signaling, function, or even development and differentiation of GC.

STAR METHODS

Detailed methods are provided in the online version of this paper and include the following:

- KEY RESOURCES TABLE
- RESOURCE AVAILABILITY
  - Lead contact
  - Materials availability
  - Data and code availability
- EXPERIMENTAL MODEL AND SUBJECT DETAILS
  - Plant materials and growth conditions
- METHOD DETAILS
  - Preparation of Arabidopsis GCP and MCP
  - Preparation of Arabidopsis root cell fluorescent protoplasts
  - Preparation of fluorescent protoplasts of rice root cells
  - Protein extraction and digestion
  - LC-MS/MS analysis of proteome
  - Proteomics data analysis
  - Un-targeted metabolomics analysis
  - Stomatal bioassay
  - Protein purification and in vitro kinase assay
  - Protoplast isolation and transactivation assay
- QUANTIFICATION AND STATISTICAL ANALYSIS
  - General statistical analysis
  - Proteomics data analysis.

- Metabolomics analysis

SUPPLEMENTAL INFORMATION

Supplemental Figure 1. Identified protein/peptide from GCP by Gdn-Cl and SLS-SDC methods.

Supplemental Figure 2. The enriched GO terms in the proteomes of *DR5 rev::GFP* and *pOs01g0248900::VENUS-N7* root cells.

Supplemental Figure 3. GO enrichment analysis of proteins enriched in GCP and MCP.

Supplemental Figure 4. Phenylpropane and cutin biosynthesis pathway in MCP and GCP.

Supplemental Figure 5. RAF15 phosphorylate SnRK2.6/OST.

Supplemental Dataset 1. Proteins identified from proteome from 250 to 10,000 GCP by Gdn-Cl and SLS-SDC methods.

Supplemental Dataset 2. Proteins identified from fluorescent protoplasts of *DR5 rev::GFP* root cells.

Supplemental Dataset 3. Proteins identified from fluorescent protoplasts of *pOs01g0248900::VENUS-N7* root cells.

Supplemental Dataset 4. All peptides identified in GCP.

Supplemental Dataset 5. All peptides identified in MCP.

Supplemental Dataset 6. Quantitative data of proteins identified in GCP and MCP.

Supplemental Dataset 7. GCP enriched proteins identified in this study.

Supplemental Dataset 8. MCP enriched proteins identified in this study.

Supplemental Dataset 9. GO analysis of proteins enriched in GCP and MCP.

Supplemental Dataset 10. The metabolomes of GCP and MCP.

Supplemental Dataset 11. Sequence of primers used in this study.

ACKNOWLEDGEMENTS

This work was supported by the Strategic Priority Research Program of the Chinese Academy of Sciences, Grant XDB27040106 (to P.W.), and National Natural Science Foundation of China, Grant 31771358 (to P.W.). We are grateful to Drs. Julian Schroeder of University of California, San Diego, for providing the seeds of *pGC1::GFP* transgenic plants, Jiawei Wang of CAS Center for Excellence in Molecular Plant Sciences for providing the seeds of *pOs01g0248900::VENUS-N7*, Zhaojun Ding of Shandong University for providing the seeds of *WOX5::ERGFP* and *DR5 rev::GFP* transgenic plants. We thank Life Science Editors for editing services.

AUTHOR CONTRIBUTIONS

P.W. designed the research. H.W., J.R. and Q.G. performed research. H.W., R.L., T.S., C.K., S.D., and C.-P.S. performed data analysis. H.W., R.L., C.K., C.-C.H., and C.-P.S. wrote the manuscript.

DELARATION OF INTERESTS

The authors declare no competing interests.

Figure Legends

Figure 1. The cell-sorting-based nano-scale pipeline for isolating and proteomic analysis of guard cell protoplasts. a. Workflow of the cell-sorting-based nanoscale pipeline for single-cell (type) proteomics. The fluorescent protoplasts were sorted by cytometry after enzymatic digestion and filtration. Protein extraction and trypsin digestion were performed in a single microcentrifuge tube, and after desalting through the C18 Stage-Tip, the peptides were subjected to LC-MS/MS. **b.** Fluorescent images showing the GFP fluorescence of *pGC1::GFP* transgenic leaves (left, Bar=50 μm) and sorted GCPs (right, Bar=50 μm). **c.** Representative flow cytometry scatter plots for *pGC1::GFP* (left) and wild type control (WT, right). **d.** The number of peptides (left) and proteins (right) identified from the indicated number of GCPs. **f.** Heatmap showing the number of peptides in each protein detected by SLS-SDC or Gdn-Cl buffers from the indicated number of GCPs.

Figure 2. Proteomic analysis of *DR5 rev::GFP* and *pOs01g0248900::VENUS-N7* fluorescent protoplasts. a. Image showing the fluorescence of *DR5 rev::GFP* transgenic seedling roots. Bar=50 μm. **b.** Representative flow cytometry scatter plots for *DR5 rev::GFP* (left) and wild type control (right). **c.** The number of peptides and proteins identified from approximately 1,000 *DR5-rev::GFP* fluorescent protoplasts. **d.** Image showing the fluorescence of root in *pOs01g0248900::VENUS-N7* transgenic rice seedling. Bar=50 μm. **e.** Representative flow cytometry scatter plots for *pOs01g0248900::VENUS-N7* (left) and wild type (WT, right). **f.** The number of peptides and proteins identified from approximately 1,000 *pOs01g0248900::VENUS-N7* transgenic rice fluorescent protoplasts.

Figure 3. Quantitative comparison of GCP and MCP proteome. a. Venn diagram showing the overlap between the proteins and peptides identified from GCP and MCP proteomes. **b.** Volcano plot of differentially up-regulated (upper panel) or down-regulated (bottom panel) proteins in the proteome of GCPs and MCPs. On the y-axis, the negative log10 values are plotted. On the x-axis, the log2 values of the fold change are seen in the comparison. **c.** Heatmap showing the quantitative comparison of proteins in GCP and MCP proteomes. **d**. Some known proteins that function in GC development are present in the proteome of GCP. **e**. Some known proteins that function in the regulation of GC intensity are present in the proteome of GCP. Yellow circles highlight proteins detected in GCPs. **f.** Some known proteins that function in stomatal movement in response to ABA, CO_2 and blue light (BL) are enriched in GCPs. All proteins listed in this panel show higher abundance in GCPs than that in MCPs (FC > 2, $p < 0.05$). **g.** Cnetplot generated by ClusterProfiler indicating proteins associated with enriched KEGG pathways; dots in light brown represent KEGG pathways, with the size of dots determined by the number of proteins belonging to the pathway. Small dots of the same size represent proteins, the dot color is determined by fold changes of protein abundance of GCP/MCP.

Figure 4. Quantitative comparison of GCP and MCP metabolome. a. PCA analysis of metabolome of the 11 MCP and 11 GCP samples. **b.** Heatmap showing the quantitative comparison of metabolites in GCP and MCP metabolome. **c.** Volcano plot showing the quantitative comparison of metabolites in GCP and MCP metabolome. **d.** Pathway analysis of

metabolites differentially accumulated in GCP and MCP. **e.** The protein-metabolite joint pathway analysis of phenylalanine/flavonoid metabolism between GCP and MCP. The metabolites, proteins, and their relationships are derived from the phenylpropanoid biosynthesis pathway (ath:00940) and the flavonoid biosynthesis pathway (ath:00941) in the KEGG database. The enzymes enriched in GCP or MCP, respectively, are colored with red or blue. Grey indicates that the enzyme has not been detected by proteomics, but it is indispensable in phenylpropane metabolism pathway.

Figure 5. RAF15 mediated SnRK2.6/OST1 activation and ABA signaling in GC. a. Presence of ABA signaling components in the GC and MC proteomes. **b.** Relative protein abundance of ABA receptor PYR1/PYLs, PP2C phosphatases, and SnRK2s in the GC and MC proteomes. **c.** Relative protein abundance of B and C subgroup RAFs in the GC and MC proteomes. **d.** Activation of the reporter gene by the combinations of RAFs with SnRK2.6 in the protoplasts of *OK*^{100}*-nonu*. The ratio of *RD29B-LUC* expression in the protoplasts with 5 μM ABA relative to that without ABA treatment was used to indicate the activation activity of different RAFs on SnRK2.6. Error bars, SEM (n = 6 individual transfections). **e.** Recombinant full-length RAF was used to phosphorylate SnRK2.6^{KR} (SnRK2.6^{K50R}, a kinase-dead form of SnRK2.6), in the presence of [γ-^{32}p]ATP. Autoradiograph (upper) and Coomassie staining (bottom) show phosphorylation and loading, respectively, of purified GST-HT1/RAF19, GST-MRK1/RAF48, GST-BHP/RAF27, GST-RAF38, HIS-RAF15, and HIS-SnRK2.6^{KR}. **f.** Ser175Ala mutation abolished RAF15 phosphorylation on SnRK2.6^{KR}. Recombinant full-length HIS-RAF15 was used to phosphorylate HIS-SnRK2.6^{KR},

SnRK2.6^{KR} with Ser171Ala mutation (SnRK2.6$^{KR\text{-}S171A}$), SnRK2.6^{KR} with Ser175Ala mutation (SnRK2.6$^{KR\text{-}S175A}$), or SnRK2.6^{KR} proteins with Ser171AlaSer175Ala mutations (SnRK2.6$^{KR\text{-}AA}$), in the presence of [γ-^{32}p]ATP. Autoradiograph (upper) and Coomassie staining (bottom) show phosphorylation and loading, respectively, of purified RAF and HIS-SnRK2.6^{KR}. **g.** RAF15-KD triggers the autophosphorylation of pre-dephosphorylated GST-SnRK2.6^{M94G} (de-SnRK2.6^{M94G}). Anti γ-S immunoblot (upper) and Coomassie staining (lower) show thiophosphorylation and loading, respectively, of recombinant GST-RAF15-KD and GST-SnRK2.6^{M94G}. **h.** RAF15-KD activates pre-dephosphorylated GST-SnRK2.6^{M94G} (de-SnRK2.6^{M94G}) and the reactivated SnRK2.6^{M94G} phosphorylates itself and ABF2. Anti γ-S immunoblot (left) and Coomassie staining (right) show thiophosphorylation and loading, respectively, of recombinant GST-RAF15-KD, GST-SnRK2.6^{M94G}, and GST-ABF2. Images shown are representative of at least two independent experiments. **i.** RAF13-KD, but not HT1, triggers the autophosphorylation of pre-dephosphorylated GST-SnRK2.6^{M94G} (de-SnRK2.6^{M94G}). Anti γ-S immunoblot (upper) and Coomassie staining (lower) show thiophosphorylation and loading, respectively, of recombinant GST-RAF13-KD, GST-HT1/RAF19-KD and GST-SnRK2.6^{M94G}. **j.** Stomatal closure of 4-week-old wild type and *raf15* mutants in response to ABA. Error bars, SD (n = 176 to 210 individual stomates). Unpaired two-tailed *t*-tests, *** $p < 0.001$. Box and whisker: 10–90 percentiles. **k.** Model showing the different RAFs mediate ABA signaling by phosphorylating SnRK2s in different cell type.

References

1. Shaw, R., Tian, X., and Xu, J. (2021). Single-Cell Transcriptome Analysis in Plants: Advances and Challenges. Mol Plant *14*, 115-126. 10.1016/j.molp.2020.10.012.
2. Rich-Griffin, C., Stechemesser, A., Finch, J., Lucas, E., Ott, S., and Schäfer, P. (2020). Single-Cell Transcriptomics: A High-Resolution Avenue for Plant Functional Genomics. Trends Plant Sci *25*, 186-197. 10.1016/j.tplants.2019.10.008.
3. de Souza, L.P., Borghi, M., and Fernie, A. (2020). Plant Single-Cell Metabolomics-Challenges and Perspectives. Int J Mol Sci *21*. 10.3390/ijms21238987.
4. Petelski, A.A., Emmott, E., Leduc, A., Huffman, R.G., Specht, H., Perlman, D.H., and Slavov, N. (2021). Multiplexed single-cell proteomics using SCoPE2. bioRxiv, 2021.2003.2012.435034. 10.1101/2021.03.12.435034.
5. Brunner, A.-D., Thielert, M., Vasilopoulou, C.G., Ammar, C., Coscia, F., Mund, A., Hoerning, O.B., Bache, N., Apalategui, A., Lubeck, M., et al. (2021). Ultra-high sensitivity mass spectrometry quantifies single-cell proteome changes upon perturbation. bioRxiv, 2020.2012.2022.423933. 10.1101/2020.12.22.423933.
6. Marx, V. (2019). A dream of single-cell proteomics. Nat Methods *16*, 809-812. 10.1038/s41592-019-0540-6.
7. Dai, S., and Chen, S. (2012). Single-cell-type proteomics: toward a holistic understanding of plant function. Mol Cell Proteomics *11*, 1622-1630. 10.1074/mcp.R112.021550.
8. Holmes-Davis, R., Tanaka, C.K., Vensel, W.H., Hurkman, W.J., and McCormick, S. (2005). Proteome mapping of mature pollen of Arabidopsis thaliana. Proteomics *5*, 4864-4884. 10.1002/pmic.200402011.
9. Noir, S., Bräutigam, A., Colby, T., Schmidt, J., and Panstruga, R. (2005). A reference map of the Arabidopsis thaliana mature pollen proteome. Biochem Biophys Res Commun *337*, 1257-1266. 10.1016/j.bbrc.2005.09.185.
10. Dai, S., Chen, T., Chong, K., Xue, Y., Liu, S., and Wang, T. (2007). Proteomics identification of differentially expressed proteins associated with pollen germination and tube growth reveals characteristics of germinated Oryza sativa pollen. Mol Cell Proteomics *6*, 207-230. 10.1074/mcp.M600146-MCP200.
11. Fíla, J., Radau, S., Matros, A., Hartmann, A., Scholz, U., Feciková, J., Mock, H.P., Čapková, V., Zahedi, R.P., and Honys, D. (2016). Phosphoproteomics Profiling of Tobacco Mature Pollen and Pollen Activated in vitro. Mol Cell Proteomics *15*, 1338-1350. 10.1074/mcp.M115.051672.
12. Zhu, M., Dai, S., McClung, S., Yan, X., and Chen, S. (2009). Functional differentiation of Brassica napus guard cells and mesophyll cells revealed by comparative proteomics. Mol Cell Proteomics *8*, 752-766. 10.1074/mcp.M800343-MCP200.
13. Zhao, Z., Zhang, W., Stanley, B.A., and Assmann, S.M. (2008). Functional Proteomics of Arabidopsis thaliana Guard Cells Uncovers New Stomatal Signaling Pathways. Plant Cell, tpc.108.063263. 10.1105/tpc.108.063263.
14. Zhang, X., Facette, M., Humphries, J.A., Shen, Z., Park, Y., Sutimantanapi, D., Sylvester, A.W., Briggs, S.P., and Smith, L.G. (2012). Identification of PAN2 by quantitative proteomics as a leucine-rich repeat-receptor-like kinase acting upstream of PAN1 to polarize cell division in maize. Plant Cell *24*, 4577-4589. 10.1105/tpc.112.104125.
15. Balmant, K.M., Lawrence, S.R., 2nd, Duong, B.V., Zhu, F., Zhu, N., Nicklay, J., and Chen, S. (2021). Guard

513 cell redox proteomics reveals a role of lipid transfer protein in plant defense. J Proteomics *242*, 104247.
514 10.1016/j.jprot.2021.104247.
515 16. Petricka, J.J., Schauer, M.A., Megraw, M., Breakfield, N.W., Thompson, J.W., Georgiev, S., Soderblom,
516 E.J., Ohler, U., Moseley, M.A., Grossniklaus, U., and Benfey, P.N. (2012). The protein expression
517 landscape of the Arabidopsis root. Proceedings of the National Academy of Sciences *109*,
518 6811-6818. 10.1073/pnas.1202546109.
519 17. Fukao, Y., Kobayashi, M., Zargar, S.M., Kurata, R., Fukui, R., Mori, I.C., and Ogata, Y. (2016). Quantitative
520 Proteomic Analysis of the Response to Zinc, Magnesium, and Calcium Deficiency in Specific Cell Types
521 of Arabidopsis Roots. Proteomes *4*, 1.
522 18. Yang, Y., Costa, A., Leonhardt, N., Siegel, R.S., and Schroeder, J.I. (2008). Isolation of a strong
523 Arabidopsis guard cell promoter and its potential as a research tool. Plant Methods *4*, 6.
524 10.1186/1746-4811-4-6.
525 19. Wang, P., Zhao, Y., Li, Z., Hsu, C.-C., Liu, X., Fu, L., Hou, Y.-J., Du, Y., Xie, S., Zhang, C., et al. (2018).
526 Reciprocal Regulation of the TOR Kinase and ABA Receptor Balances Plant Growth and Stress
527 Response. Molecular Cell *69*, 100-112.e106. 10.1016/j.molcel.2017.12.002.
528 20. Hsu, C.-C., Zhu, Y., Arrington, J.V., Paez, J.S., Wang, P., Zhu, P., Chen, I.-H., Zhu, J.-K., and Tao, W.A.
529 (2018). Universal Plant Phosphoproteomics Workflow and Its Application to Tomato Signaling in
530 Response to Cold Stress*. Molecular Cellular Proteomics *17*, 2068-2080. 10.1074/mcp.TIR118.000702.
531 21. Benková, E., Michniewicz, M., Sauer, M., Teichmann, T., Seifertová, D., Jürgens, G., and Friml, J. (2003).
532 Local, Efflux-Dependent Auxin Gradients as a Common Module for Plant Organ Formation. Cell *115*,
533 591-602. https://doi.org/10.1016/S0092-8674(03)00924-3.
534 22. Zhang, T.-Q., Chen, Y., Liu, Y., Lin, W.-H., and Wang, J.-W. (2021). Single-cell transcriptome atlas and
535 chromatin accessibility landscape reveal differentiation trajectories in the rice root. Nature
536 Communications *12*, 2053. 10.1038/s41467-021-22352-4.
537 23. Ohashi-Ito, K., and Bergmann, D.C. (2006). Arabidopsis FAMA controls the final
538 proliferation/differentiation switch during stomatal development. Plant Cell *18*, 2493-2505.
539 10.1105/tpc.106.046136.
540 24. Chen, L., Guan, L., Qian, P., Xu, F., Wu, Z., Wu, Y., He, K., Gou, X., Li, J., and Hou, S. (2016). NRPB3, the
541 third largest subunit of RNA polymerase II, is essential for stomatal patterning and differentiation in
542 Arabidopsis. Development *143*, 1600-1611. 10.1242/dev.129098.
543 25. Negi, J., Moriwaki, K., Konishi, M., Yokoyama, R., Nakano, T., Kusumi, K., Hashimoto-Sugimoto, M.,
544 Schroeder, J.I., Nishitani, K., Yanagisawa, S., and Iba, K. (2013). A Dof transcription factor, SCAP1, is
545 essential for the development of functional stomata in Arabidopsis. Curr Biol *23*, 479-484.
546 10.1016/j.cub.2013.02.001.
547 26. Hu, H., Boisson-Dernier, A., Israelsson-Nordstrom, M., Bohmer, M., Xue, S., Ries, A., Godoski, J., Kuhn,
548 J.M., and Schroeder, J.I. (2010). Carbonic anhydrases are upstream regulators of CO2-controlled
549 stomatal movements in guard cells. Nat Cell Biol *12*, 87-93.
550 http://www.nature.com/ncb/journal/v12/n1/suppinfo/ncb2009_S1.html.
551 27. Hashimoto, M., Negi, J., Young, J., Israelsson, M., Schroeder, J.I., and Iba, K. (2006). Arabidopsis HT1
552 kinase controls stomatal movements in response to CO2. Nat Cell Biol *8*, 391-397. 10.1038/ncb1387.
553 28. Hiyama, A., Takemiya, A., Munemasa, S., Okuma, E., Sugiyama, N., Tada, Y., Murata, Y., and Shimazaki,
554 K.I. (2017). Blue light and CO(2) signals converge to regulate light-induced stomatal opening. Nat
555 Commun *8*, 1284. 10.1038/s41467-017-01237-5.
556 29. Kinoshita, T., Doi, M., Suetsugu, N., Kagawa, T., Wada, M., and Shimazaki, K. (2001). Phot1 and phot2

557 mediate blue light regulation of stomatal opening. Nature *414*, 656-660. 10.1038/414656a.
558 30. Takemiya, A., Sugiyama, N., Fujimoto, H., Tsutsumi, T., Yamauchi, S., Hiyama, A., Tada, Y., Christie, J.M.,
559 and Shimazaki, K. (2013). Phosphorylation of BLUS1 kinase by phototropins is a primary step in
560 stomatal opening. Nat Commun *4*, 2094. 10.1038/ncomms3094.
561 31. Hayashi, M., Inoue, S.I., Ueno, Y., and Kinoshita, T. (2017). A Raf-like protein kinase BHP mediates blue
562 light-dependent stomatal opening. Sci Rep *7*, 45586. 10.1038/srep45586.
563 32. Flütsch, S., Wang, Y., Takemiya, A., Vialet-Chabrand, S.R.M., Klejchová, M., Nigro, A., Hills, A., Lawson,
564 T., Blatt, M.R., and Santelia, D. (2020). Guard Cell Starch Degradation Yields Glucose for Rapid Stomatal
565 Opening in Arabidopsis. Plant Cell *32*, 2325-2344. 10.1105/tpc.18.00802.
566 33. Lee, M., Choi, Y., Burla, B., Kim, Y.-Y., Jeon, B., Maeshima, M., Yoo, J.-Y., Martinoia, E., and Lee, Y. (2008).
567 The ABC transporter AtABCB14 is a malate importer and modulates stomatal response to CO2. Nat
568 Cell Biol *10*, 1217-1223.
569 http://www.aginternetwork.net/whalecomwww.nature.com/whalecom0/ncb/journal/v10/n10/suppi
570 nfo/ncb1782_S1.html.
571 34. Watkins, J.M., Chapman, J.M., and Muday, G.K. (2017). Abscisic Acid-Induced Reactive Oxygen Species
572 Are Modulated by Flavonols to Control Stomata Aperture. Plant Physiol *175*, 1807-1825.
573 10.1104/pp.17.01010.
574 35. Watkins, J.M., Hechler, P.J., and Muday, G.K. (2014). Ethylene-induced flavonol accumulation in guard
575 cells suppresses reactive oxygen species and moderates stomatal aperture. Plant Physiol *164*,
576 1707-1717. 10.1104/pp.113.233528.
577 36. Medeiros, D.B., Barros, J.A.S., Fernie, A.R., and Araújo, W.L. (2020). Eating Away at ROS to Regulate
578 Stomatal Opening. Trends Plant Sci *25*, 220-223. 10.1016/j.tplants.2019.12.023.
579 37. Amsbury, S., Hunt, L., Elhaddad, N., Baillie, A., Lundgren, M., Verhertbruggen, Y., Scheller, Henrik V.,
580 Knox, J.P., Fleming, Andrew J., and Gray, Julie E. (2016). Stomatal Function Requires Pectin
581 De-methyl-esterification of the Guard Cell Wall. Current Biology *26*, 2899-2906.
582 10.1016/j.cub.2016.08.021.
583 38. Li, Y., Beisson, F., Koo, A.J., Molina, I., Pollard, M., and Ohlrogge, J. (2007). Identification of
584 acyltransferases required for cutin biosynthesis and production of cutin with suberin-like monomers.
585 Proc Natl Acad Sci U S A *104*, 18339-18344. 10.1073/pnas.0706984104.
586 39. Lin, Z., Li, Y., Zhang, Z., Liu, X., Hsu, C.-C., Du, Y., Sang, T., Zhu, C., Wang, Y., Satheesh, V., et al. (2020). A
587 RAF-SnRK2 kinase cascade mediates early osmotic stress signaling in higher plants. Nature
588 Communications *11*, 613. 10.1038/s41467-020-14477-9.
589 40. Takahashi, Y., Zhang, J., Hsu, P.-K., Ceciliato, P.H.O., Zhang, L., Dubeaux, G., Munemasa, S., Ge, C., Zhao,
590 Y., Hauser, F., and Schroeder, J.I. (2020). MAP3Kinase-dependent SnRK2-kinase activation is required
591 for abscisic acid signal transduction and rapid osmotic stress response. Nature Communications *11*, 12.
592 10.1038/s41467-019-13875-y.
593 41. Lin, Z., Li, Y., Wang, Y., Liu, X., Ma, L., Zhang, Z., Mu, C., Zhang, Y., Peng, L., Xie, S., et al. (2021).
594 Initiation and amplification of SnRK2 activation in abscisic acid signaling. Nature Communications *12*,
595 2456. 10.1038/s41467-021-22812-x.
596 42. Ng, L.M., Soon, F.F., Zhou, X.E., West, G.M., Kovach, A., Suino-Powell, K.M., Chalmers, M.J., Li, J., Yong,
597 E.L., Zhu, J.K., et al. (2011). Structural basis for basal activity and autoactivation of abscisic acid (ABA)
598 signaling SnRK2 kinases. Proceedings of the National Academy of Sciences of the United States of
599 America *108*, 21259-21264. 10.1073/pnas.1118651109.
600 43. Vlad, F., Droillard, M.-J., Valot, B., Khafif, M., Rodrigues, A., Brault, M., Zivy, M., Rodriguez, P.L., Merlot,

601 S., and Laurière, C. (2010). Phospho-site mapping, genetic and in planta activation studies reveal key
602 aspects of the different phosphorylation mechanisms involved in activation of SnRK2s. The Plant
603 Journal *63*, 778-790.
604 44. Jin, X., Wang, R.-S., Zhu, M., Jeon, B.W., Albert, R., Chen, S., and Assmann, S.M. (2013). Abscisic
605 acid-responsive guard cell metabolomes of Arabidopsis wild-type and gpa1 G-protein mutants. The
606 Plant cell *25*, 4789-4811. 10.1105/tpc.113.119800.
607 45. Lundberg, E., and Borner, G.H.H. (2019). Spatial proteomics: a powerful discovery tool for cell biology.
608 Nat Rev Mol Cell Biol *20*, 285-302. 10.1038/s41580-018-0094-y.
609 46. Mustilli, A.-C., Merlot, S., Vavasseur, A., Fenzi, F., and Giraudat, J. (2002). Arabidopsis OST1 Protein
610 Kinase Mediates the Regulation of Stomatal Aperture by Abscisic Acid and Acts Upstream of Reactive
611 Oxygen Species Production. THE PLANT CELL *14*, 3089-3099.
612 47. Melotto, M., Underwood, W., Koczan, J., Nomura, K., and He, S.Y. (2006). Plant Stomata Function in
613 Innate Immunity against Bacterial Invasion. Cell *126*, 969-980.
614 48. Vlad, F., Rubio, S., Rodrigues, A., Sirichandra, C., Belin, C., Robert, N., Leung, J., Rodriguez, P.L., Lauriere,
615 C., and Merlot, S. (2009). Protein phosphatases 2C regulate the activation of the Snf1-related kinase
616 OST1 by abscisic acid in Arabidopsis. Plant Cell *21*, 3170-3184. 10.1105/tpc.109.069179.
617 49. Fujii, H., Chinnusamy, V., Rodrigues, A., Rubio, S., Antoni, R., Park, S.-Y., Cutler, S.R., Sheen, J.,
618 Rodriguez, P.L., and Zhu, J.-K. (2009). In vitro reconstitution of an abscisic acid signalling pathway.
619 Nature *462*, 660-664.
620 50. Ma, Y., Szostkiewicz, I., Korte, A., Moes, D., Yang, Y., Christmann, A., and Grill, E. (2009). Regulators of
621 PP2C Phosphatase Activity Function as Abscisic Acid Sensors. Science *324*, 1064-1068.
622 10.1126/science.1172408.
623 51. Miyazono, K.-i., Miyakawa, T., Sawano, Y., Kubota, K., Kang, H.-J., Asano, A., Miyauchi, Y., Takahashi, M.,
624 Zhi, Y., Fujita, Y., et al. (2009). Structural basis of abscisic acid signalling. Nature *462*, 609-614.
625 52. Park, S.-Y., Fung, P., Nishimura, N., Jensen, D.R., Fujii, H., Zhao, Y., Lumba, S., Santiago, J., Rodrigues, A.,
626 Chow, T.-f.F., et al. (2009). Abscisic Acid Inhibits Type 2C Protein Phosphatases via the PYR/PYL Family
627 of START Proteins. Science *324*, 1068-1071. 10.1126/science.1173041.
628 53. Soma, F., Takahashi, F., Suzuki, T., Shinozaki, K., and Yamaguchi-Shinozaki, K. (2020). Plant Raf-like
629 kinases regulate the mRNA population upstream of ABA-unresponsive SnRK2 kinases under drought
630 stress. Nature Communications *11*, 1373. 10.1038/s41467-020-15239-3.
631 54. Hsu, P.K., Takahashi, Y., Merilo, E., Costa, A., Zhang, L., Kernig, K., Lee, K.H., and Schroeder, J.I. (2021).
632 Raf-like kinases and receptor-like (pseudo)kinase GHR1 are required for stomatal vapor pressure
633 difference response. Proc Natl Acad Sci U S A *118*. 10.1073/pnas.2107280118.
634
635

STAR Methods

KEY RESOURCES TABLE

REAGENT or RESOURCE	SOURCE	IDENTIFIER
Antibodies		
Anti-thiophosphate ester	Abcam	Cat#ab92570
Anti-actin	ABclonal	Cat#AC009
Bacterial and virus stains		
Escherichia coli DH5a	Widely dist	N/A
Arctic Express	Thermo Fis Scientific	Cat#CY50905
BL21 DE3	Widely dist	N/A
Chemicals, peptides, and recombinant proteins		
Abscisic Acid	Sigma-Aldr	Cat#A1049
Luciferase Assay Reagent	Promega	Cat#E1483
Cellulose R10	Yakult Pharmaceut Industry	Lot#210824-01
Cellulose Onozuka RS	Yakult Pharmaceut Industry	Lot#200116-01
Macrozyme R10	Yakult Pharmaceut Industry	Lot#210317-01
Pectolyase Y-23	Yakult Pharmaceut Industry	Cat#Y-011
Polyvinyl pyrrolidone 40,000	Sigma-Aldr	Cat#V900008
MES	Sigma-Aldr	Cat#M3671
Sorbitol	Sigma-Aldr	Cat#S1876
Mannitol	Sigma-Aldr	Cat#M9647
Sodium lauroyl sarcosinate	Sigma-Aldr	Cat#L5777
Sodium deoxycholate	Sigma-Aldr	Cat#30970
Bovine serum albumin	Yeasen Bio	Cat#36101ES60
L-ascorbic acid	Sigma-Aldr	Cat#95209
TCEP	Sigma-Aldr	Cat#C4706
TEAB	Sigma-Aldr	Cat#T7408
Trypsin	Promega	Cat#V5113
Guanidine chloride	Sigma-Aldr	Cat#G3272
CAA	Sigma-Aldr	Cat#C0267
Formic acid	Merck	Cat#5.43804
Acetonitrile	Honeywell	Cat#34967
C^{18} resin	CDS Analy	Cat#2240

	LLC Headq	
Lambda Protein Phosphatase	NEB	Cat#P0753S
Glutathione Sepharose	Cytiva	Cat#17513202
$CaCl_2$	Sigma-Aldr	Cat#C7902
KCl	Sigma-Aldr	Cat#P3911
$MgCl_2$	Sigma-Aldr	Cat#M9272
β-Mercaptoethanol	Sigma-Aldr	Cat#M6250
PEG4000	Sigma-Aldr	Lot#BCBZ5475
Trans-1,2-diaminocyclo-hexane-N,N,N',N',-tetraacetic acid (DACTAA)	Sigma-Aldr	Cat#D-1383
4-methylumbelliferyl glucuronide (MUG)	Gold Bio Technology	Cat#MUG-1G
Triton X-100	Sigma-Aldr	Cat#T-8787
DTT	Sigma-Aldr	Cat#D-9779
Na_2CO_3	Sigma-Aldr	Cat#S7795
γ-^{32}P-ATP	PerkinElme	Cat#NEG502Z500UC
N^6-Benzyl-ATPγS	Abcam	Cat#ab138911
p-nitrobenzyl mesylate	Abcam	Cat#ab138910
Deposited Data		
Raw Imaging Files	This study, Mendeley I	doi:10.17632/2zchtvbv58.1
Experimental Models: Organisms/strains		
pGC1::GFP	Yang et al.	N/A
DR5rev::GFP	Benková et	N/A
pOs01g0248900::VENUS-N7	Zhang et al.	N/A
OK^{100}-nonu	Lin et al.[39]	N/A
raf15-1	This study	Salk_020351
raf15-2	This study	Salk_044414
Recombinant DNA		
RD29B-LUC	Lin et al.[41]	N/A
ZmUBQ-GUS	Lin et al.[41]	N/A
pSAT6-FLAG	Lin et al.[41]	N/A
pSAT6-AT1G62400-FLAG	This study	N/A
pSAT6-AT3G01490-FLAG	This study	N/A
pSAT6-AT3G58640-FLAG	This study	N/A
pSAT6-AT3G63260-FLAG	This study	N/A
pSAT6-AT4G18950-FLAG	This study	N/A
pSAT6-AT4G31170-FLAG	This study	N/A
pSAT6-AT5G50000-FLAG	This study	N/A
pSAT6-AT1G62400^{K113R}-FLAG	This study	N/A
pSAT6-AT3G58640^{K580R}-FLAG	This study	N/A

pGEX-4T-1-1G62400	This study	N/A
pGEX-4T-1-3G01490	This study	N/A
pGEX-4T-1-3G63260	This study	N/A
pGEX-4T-1-4G18950	This study	N/A
pGEX-4T-1-4G31170	This study	N/A
pGEX-4T-1-5G50000	This study	N/A
pGEX-4T-1-3G58640-KD	This study	N/A
pET-28a-3G58640	This study	N/A
pET-28a-SnRK2.6^{K50R}	Lin et al.[41]	N/A
pET-28a-SnRK2.6$^{K50R\text{-}S171A}$	Lin et al.[41]	N/A
pET-28a-SnRK2.6$^{K50R\text{-}S175A}$	Lin et al.[41]	N/A
pET-28a-SnRK2.6$^{K50R\text{-}AA}$	Lin et al.[41]	N/A
pGEX-4T-1-SnRK2.6^{M94G}	Lin et al.[41]	N/A
pET-28a-SnRK2.4^{K33R}	Lin et al.[41]	N/A
pGEX-4T-1-ABF2	Lin et al.[41]	N/A
pGEX-4T-1-2G31010-KD	This study	N/A
pGEX-4T-1-2G42640-KD	This study	N/A
Oligonucleotides		
Primers provided in Dataset 11		
Software		
Proteome Discoverer Version 2.4	Thermo Fis Scientific	N/A
Compound Discoverer Version 3.2	Thermo Fis Scientific	N/A
EXCEL software	Microsoft	N/A
Prism 9.3.0	GraphPad	N/A
Western Blot Touch Imager System	E-BLOT	N/A

RESOURCE AVAILABILITY

Lead contact

Further information and requests for resources and reagents should be directed to and will be fulfilled by the Lead Contact, Pengcheng Wang (pcwang@cemps.ac.cn).

Materials availability

Plasmids and plant materials generated in this study are all available from the Lead Contact upon request.

Data and code availability

- The proteomics data were deposited to the ProteomeXchange Consortium with the dataset identifier PXD030489 and PXD030511, the metabolomics data were deposited to MetaboLights with dataset identifier MTBLS3997.
- Any additional information required to reanalyze the data reported in this paper is available from the lead contact upon request.
-

EXPERIMENTAl MODEL AND SUBJECT DETAILS

Growth conditions and plant materials. The *pGC1::GFP* [18] and *DR5rev::GFP* [21] seeds were sterilized in 75% ethanol and germinated on half-strength Murashige and Skoog (MS) medium plates with 0.75 agar. After 7 days' growth on the plates, the *pGC1::GFP* seedlings were transplanted to soil, and rosette leaves were harvested at the indicated time for protoplast isolation.

The seeds of *pOs01g0248900::VENUS-N7* transgenic rice [22] were grown in a half-strength MS liquid medium in the growth chamber at 26 °C with 60% humidity (16 h light/8 h dark). After 7 days, the root tips of the seedlings were harvested for protoplast isolation.

METHOD DETAILS

Preparation of *Arabidopsis* GCP and MCP. The rosette leaves of three-week-old seedlings of *pGC1::GFP* grown in the soil were blended for 10 s five times in 100 mL ice-cold water. The blended mixture was filtered through a 100 μm mesh (Falcon) to remove the broken

mesophyll and epidermal cells. The peels were transferred into 20 mL enzyme solution containing 1.35% cellulose R10 (Yakult Pharmaceutical Industry), 0.268% macrozyme R10 (Yakult Pharmaceutical Industry), 0.1% polyvinyl pyrrolidone 40,000 (PVP-40), 0.25% bovine serum albumin (BSA), 0.5 mM L-ascorbic acid, 2.75 mM 2-[N-morpholino] ethanesulfonic acid hydrate-Tris (MES), pH 5.5, 0.275 mM $CaCl_2$, 0.275 mM $MgCl_2$, 5.5 μM KH_2PO_4, and 0.275 M sorbitol at 27 °C with shaking. After 1 h digestion, the peels were filtered with 100 μm mesh and placed into 10 ml enzyme solution II containing 1.3% cellulose Onozuka RS (Yakult Pharmaceutical Industry), 0.0075% Pectolyase Y-23 (Yakult Pharmaceutical Industry), 0.25% BSA, 0.5 mM L-ascorbic acid, 5 mM MES, pH 5.5, 0.5 mM $CaCl_2$, 0.5 mM $MgCl_2$, 10 μM KH_2PO_4 and 0.5 M sorbitol at 27 °C for 2 h. The digestion mixture was filtered with 40 μm mesh (Falcon), and the GCP were collected by centrifugation at 200 × *g* for 5 min. The protoplasts were resuspended in the same solution without enzyme and sorted using cytometry (ARIA III Cell sorter, BD bioscience) with the GFP signal and single-cell pattern to isolate high purity (~ 100%) fluorescent protoplasts. The indicated number of cells were collected by centrifugation and used for protein extraction for LC-MS/MS.

For isolating Arabidopsis MCP, leaf strips were excised from the middle parts of young rosette leaves, dipped in an enzyme solution containing 1.35% cellulase R10 (Yakult Pharmaceutical Industry) and 0.268% macerozyme R10 (Yakult Pharmaceutical Industry), and incubated at room temperature in the dark. The protoplast solution was diluted with an equal volume of W5 solution (2 mM MES, pH 5.7, 154 mM NaCl, 125 mM $CaCl_2$, and 5 mM KCl) and filtered through a nylon mesh. The MCP were resuspended with 10 ml W5

buffer and sorted using cytometry (ARIA III Cell sorter, BD bioscience), using chloroplast's autofluorescence to isolate high purity (~ 100%) fluorescent protoplasts. The indicated number of cells were collected by centrifugation and used for protein extraction for LC-MS/MS.

Preparation of Arabidopsis root cell fluorescent protoplasts. To isolate *DR5 rev::GFP* fluorescent protoplasts, the root tip regions (about 0.5 cm from root tip) were cut from the roots of 7-day-old Arabidopsis seedling. The root tips were digested for 2 h in enzyme solution containing 1.5% cellulase R10, 1.5% macerozyme R10, 0.4 M mannitol, 10 mM KCl, 10 mM $CaCl_2$ and 0.1% BSA. The protoplasts were filtered with a 40 μm mesh (Falcon) and centrifuged at 500 × *g* for 6 min. The protoplasts were resuspended in 8% mannitol and sorted using cytometry (FACS ARIA III Cell sorter, BD bioscience) with the GFP signal and single-cell pattern to isolate high purity (~ 100%) fluorescent protoplasts. The indicated number of cells were collected by centrifugation and used for protein extraction for LC-MS/MS.

Preparation of fluorescent protoplasts of rice root cells. The root tips of 6-day old rice seedlings were harvested and digested for 3 h at room temperature in an enzyme solution containing 4% cellulose Onozuka RS, 1.5% macerozyme R10, 0.4 M mannitol, 0.1 M MES, 10 mM KCl, 10 mM $CaCl_{2,}$ and 0.1% BSA with shaking every 30 min. The protoplasts were filtered with a 40 μm mesh (Falcon) and centrifuged at 500 × *g* for 6 min. The protoplasts were resuspended in 8% mannitol and sorted using cytometry (BD bioscience, ARIA III Cell

sorter) with the GFP signal and single-cell pattern to isolate high purity (~ 100%) fluorescent protoplasts. The indicated number of cells were collected by centrifugation and used for protein extraction for LC-MS/MS.

Protein extraction and digestion. Two sample preparation workflows were compared for the efficiency of protein extraction. GCP and MCP were lysed in SLS-SDC buffer (12 mM sodium lauroyl sarcosinate (SDS), 12 mM sodium deoxycholate (SDC), 100 mM Tris-Cl, pH 8.5) or 6 M guanidine chloride (Gdn-Cl). All the lysis chemicals were dissolved in 100 mM Tris-HCl (pH 8.5). Proteins were reduced and alkylated with 10 mM Tris (2-carboxyethyl) phosphine hydrochloride (TCEP) and 40 mM 2-Chloroacetamide (CAA) at 95 °C for 10 min. Proteins were then subjected to five cycles of ultrasonication pulses of 30 sec and pauses of 30 sec. Protein extracts were 5-fold diluted using 50 mM triethylammonium bicarbonate (TEAB), and trypsin was subsequently added to a final 1:100 (w/w) enzyme-to-protein ratio and incubated at 37 °C overnight. For the Gdn-Cl method, proteins were precipitated using methanol-chloroform precipitation, and the precipitated protein pellet was air dried. The pellet was suspended in SLS-SDC buffer and the SLS-SDC protocol for enzymatic digestion and detergent precipitation followed. For both methods, the digested peptides were desalted using a C18 StageTip.

LC-MS/MS analysis of proteome. The peptides were analyzed using Orbitrap Fusion (Thermo Fisher Scientific) or timsTOF pro (Bruker) mass spectrometer. To analyze 1 μg of GCP and MCP digests, the peptides were dissolved in 4 μL of 0.2% formic acid (FA) and

injected into an Easy-nLC 1200 (Thermo Fisher Scientific). Peptides were separated on a 15 cm in-house packed column (360 μm OD × 75 μm ID) containing C18 resin (2.2 μm, 100 Å, Michrom Bioresources). The mobile phase buffer consisted of 0.1% FA in ultra-pure water (Buffer A) with an eluting buffer of 0.1% FA in 80% ACN (Buffer B) run over a linear 182 min gradient of 5–35% buffer B at a flow rate of 300 nL/min. The Easy-nLC 1200 was coupled online with an Orbitrap Fusion Tribrid mass spectrometer. The mass spectrometer was operated in the data-dependent acquisition (DDA) mode in which a full-scan MS (from m/z 350–1500 with the resolution of 120,000) was followed by top speed higher-energy collision dissociation (HCD) MS/MS scans of the most abundant ions with dynamic exclusion for 60 s.

For the analysis of the digests of counted 250 to 10,000 GCP cells, the peptides were dissolved in 4 μL of 0.2% FA and injected into nanoflow reversed-phase chromatography, which was performed on an EASY-nLC 1200 system (Thermo Fisher Scientific). Peptides were separated in 120 min at a flow rate of 300 nl min on a 25 cm × 75 μm column with a laser-pulled electrospray emitter packed with 1.6 μm ReproSil-Pur C18-AQ particles. Mobile phases A and B were water with 0.1 % FA and 80:20:0.1 % ACN: water: FA, respectively. The fraction of B was linearly increased from 2% to 27% in 90 min, followed by an increase to 46% in 22 min and a further increase to 100% in 3 min before re-equilibration. Liquid chromatography was coupled online to a hybrid TIMS quadrupole TOF mass spectrometer (timsTOF Pro) via a CaptiveSpray nano-electrospray ion source. The electrospray voltage applied was 1.60 kV. Precursors and fragments were analyzed at the TOF detector, with a MS/MS scan range from 300 to 1500m/z. The timsTOF Pro was operated in parallel

accumulation serial fragmentation (PASEF) mode. Precursors with charge states 2 to 3 were selected for fragmentation, and 4 PASEF-MS/MS scans were acquired per cycle. The dynamic exclusion was set to 24 s.

For the analysis of the proteome of fluorescent protoplasts of *DR5 rev::GFP* and *pOs01g0248900::VENUS-N7* root cells, peptides were separated using a Thermo UltiMate 3000 RSLC nano ProFlow system (Thermo Fisher Scientific) with a gradient comprised an increase from 5% to 38% solvent buffer A (0.1% FA in water) over 80 min, 25%–38% in 15 min, increasing to 99% buffer B (80% ACN, 19.9% H_2O, 0.1% FA) over 1 min, and then holding at 99% buffer B for the last 9 min, all at a constant flow rate of 100 nL/min. Samples were separated over a 15 cm 100 C18. All samples were analyzed in a nanoscale liquid chromatography (nLC)–MS/MS analysis of 100 min using an Eclipse + FAIMS mass spectrometer (Thermo Fisher Scientific). The mass spectrometer was operated in the data-dependent mode in which a full-scan MS (from m/z 375–1500 with the Orbitrap resolution of 240,000) was followed by Cycle 3 sec higher-energy collision dissociation (HCD) MS/MS scans of the most abundant ions with dynamic exclusion for 60 s.

Un-targeted metabolomics analysis. Around 100,000 GCP and 100,000 MCP were suspended in 500 μL of extraction solution (90% methanol). After ultrasonic homogenization for 2 min and vortexing for 10 min, the samples were kept in the dark for 16 h, dried under vacuum, resuspended in 50 μL 40% methanol in water, and centrifuged at 15,000 × *g* for 30 min, 4 °C. The clear supernatants were loaded into injection vials and ready for UHPLC-MS/MS.

For UHPLC-MS/MS assay, the vanquish-flex UHPLC system was coupled to Q Exactive Plus (Thermo Fisher Scientific) for metabolite separation and detection. A Hypersil GOLD column (2.1×100 mm.1.9 um; Thermo Fisher Scientific) was employed for compound separation at 30 °C, and 1 μl of sample was loaded. The mobile phase A was HPLC grade H_2O with 0.1% (v/v) FA and phase B was HPLC grade ACN. The gradient elution conditions were set as follows: from 0 to 2 min, the mobile phase B increased to 10%; from 2 to 10 min, the mobile phase B increased to 50%; from 10 to 10.1 min the mobile phase B increased to 80%; from 10.1 to 13 min, the mobile phase B was kept at 80%; from 13 to 14 min the mobile phase B increased to 95%; from 14-18 min the mobile phase B decreased to 10%. The flow rate was 0.3 mL/min.

The MS data acquisition was performed by the Q Exactive Plus system. In full scan MS/$ddMS^2$ mode, the resolutions of full scan MS and $ddMS^2$ were set at 70,000 and 17,500, respectively. The automatic gain control (AGC) target and maximum injection time in full scan MS settings were 1^{e6} and 100 ms, while their values were 2^{e5} and 50 ms in $ddMS^2$ settings. The TopN (N, the number of top most abundant ions for fragmentation) was set to 8, and collision energy was set to 20%, 40% and 60%. A heated ESI source was used at positive and negative ion mode. The spray voltage was set as 3.5 KV for positive mode and 3.2 KV for negative mode; the capillary temperature and aux gas heater temperature were set as 320 and 350 °C, respectively. Sheath gas and aux gas flow rate were set at 35 and 15 (in arbitrary units), respectively. The S-lens RF level was 50.

Stomatal bioassay. For stomatal aperture assay, rosette leaves of 4-week-old Arabidopsis

seedlings were taken. Epidermal strips were peeled out and incubated in buffer containing 50 mM KCl and 10 mM MES, pH 6.15, in a plant growth chamber for 3 h before ABA treatment. Stomatal apertures were measured 2 h after the addition of 5 μM ABA. The apertures of indicated number of stomata per sample were measured by quantifying the pore width of stomata using Image J software. All the experiments were repeated at least three times.

Protein purification and *in vitro* kinase assay. For *in vitro* kinase assays, full length coding sequence of SnRK2.6 and kinase domains of RAFs were cloned into either *pGEX-4T-1, pET28a or pET-SUMO vectors* and transformed into BL21 or ArcticExpress cells. The recombinant proteins were expressed and purified as previously described [39]. For the phosphorylation assay, **recombinant full-length** RAF15, HT1/RAF19, MRK1/RAF48, BHP/RAF27, RAF38, and the kinase domains of RAF13 (aa 492-775) and RAF14 (aa 518-781) were incubated with "kinase-dead" forms of SnRK2.6 with or without Ser to Ala mutations at Ser171 and Ser175 in reaction buffer (25 mM Tris HCl, pH 7.4, 12 mM $MgCl_2$, 2 mM DTT), with 1 μM ATP plus 1 μCi of [γ-^{32}P] ATP for 30 min at 30°C. Reactions were stopped by boiling in SDS sample buffer and proteins were separated by 10% SDS-PAGE. Primers used in RAF construction are listed in Supplementary Dataset 11.

For the dephosphorylation assay, SnRK2.6^{M94G} coated on Glutathione Sepharose (Cytiva) were dephosphorylated with Lambda Protein Phosphatase (λPP) for 30 min and the λPP was removed by washing three times with protein buffer (25 mM Tris HCl, pH 7.4, 150 mM NaCl). To detect the effects of RAF15 on SnRK2.6^{M94G} thiophosphorylation and activity, recombinant GST-RAF15-KD (aa 548-809) was incubated with pre-dephosphorylated

822 SnRK2.6^{M94G} for 30 min in reaction buffer (25 mM Tris HCl, pH 7.4, 12 mM $MgCl_2$, 2mM
823 $MnCl_2$, 0.5 mM DTT, 50 μM ATP, 50 μM N^6-Benzyl-ATPγS). Then ABF2 was added to the
824 reaction and incubated for an additional 30 min. This phosphorylation reaction was stopped
825 by adding EDTA to a final concentration of 25 μM. A final concentration of 2.5 mM
826 p-nitrobenzyl mesylate (Abcam, ab138910) was added to proceed the alkylating reaction for
827 1 h at room temperature. Samples with SDS sample buffer were boiled and separated by
828 SDS-PAGE, transferred to Polyvinylidene fluoride (PVDF) membrane, and immunoblotted
829 with antibodies against thiophosphate ester (Abcam, ab92570).
830
831 **Protoplast isolation and transactivation assay.** Protoplast isolation and transactivation
832 assays were performed as previously described [19]. Briefly, protoplasts were isolated from
833 leaves of 4-week-old plants grown under a short photoperiod (10 h light at 23°C/14 h dark at
834 20°C). Leaf strips were excised from the middle parts of young rosette leaves, dipped in an
835 enzyme solution containing cellulase R10 (Yakult Pharmaceutical Industry) and macerozyme
836 R10 (Yakult Pharmaceutical Industry), and incubated at room temperature in the dark. The
837 protoplast solution was diluted with an equal volume of W5 solution (2 mM MES, pH 5.7,
838 154 mM NaCl, 125 mM $CaCl_2$, and 5 mM KCl) and filtered through a nylon mesh. The
839 flow-through was centrifuged at 100 *g* for 2 min to pellet the protoplasts. Protoplasts were
840 resuspended in W5 solution and incubated for 30 min. 100 μL of protoplasts suspended in
841 MMG solution (4 mM MES, pH 5.7, 0.4 M mannitol, and 15 mM $MgCl_2$) were mixed with
842 the plasmid mix and added to 110 μL PEG solution (40% w/v PEG-4000, 0.2 M mannitol,
843 and 100 mM $CaCl_2$). The transfection mixture was mixed completely by gently tapping the

tube followed by incubation at room temperature for 5 min. The protoplasts were washed twice with 1 mL W5 solution. The *RD29B-LUC* (7 μg of plasmid per transfection) and *ZmUBQ-GUS* (1 μg per transfection) were used as an ABA-responsive reporter gene and as an internal control, respectively. For wild type and mutated *RAF*, *SnRK2.6* plasmids, 3 μg per transfection were used. After transfection, protoplasts were incubated for 5 h under light in washing and incubation solution (0.5 M mannitol, 20 mM KCl, 4 mM MES, pH 5.7) with or without 5 μM ABA. The mutations were introduced into wild type RAFs using the primers listed in Supplementary Dataset 11.

Primer list

Dataset S11 presents the sequences of the primers used in this study.

QUANTIFICATION AND STATISTICAL ANALYSIS

General statistical analysis

Statistic significance of relative luciferase activity, phosphatase activity, fresh weight, Rosetta diameter, relative intensity, ion leakage, gene expression was examined by Student's t test (*$p < 0.05$, **$p < 0.01$, ***$p < 0.001$).

Proteomics data analysis

The raw files were searched directly against the Arabidopsis thaliana database (TAIR10 with 35,386 entries) with no redundant entries using SEQUEST HT search algorithm on Proteome Discoverer software (version 2.4). Peptide precursor mass tolerance was set at 10 ppm, and

MS/MS tolerance was set at 0.02 Da. Three missed cleavage sites of trypsin were allowed. Search criteria included a static carbamidomethylation of cysteine (+57.0214 Da) and variable modifications of oxidation (+15.9949 Da) on methionine and phosphorylation (+79.9663 Da) on serine, threonine, and tyrosine. The false discovery rates (FDR) of proteins and peptides were set at 1% FDR.

Metabolomics analysis

Following LC−MS analysis, raw data were collected and processed using Compound Discoverer 3.2 (Thermo Fisher Scientific) with the metabolite databases including mzCloud, mzVault, Masslist, and Chemspider. Principal component analysis (PCA), heatmap analysis of metabolites, and volcano plots were performed using R (version 4.0) software.

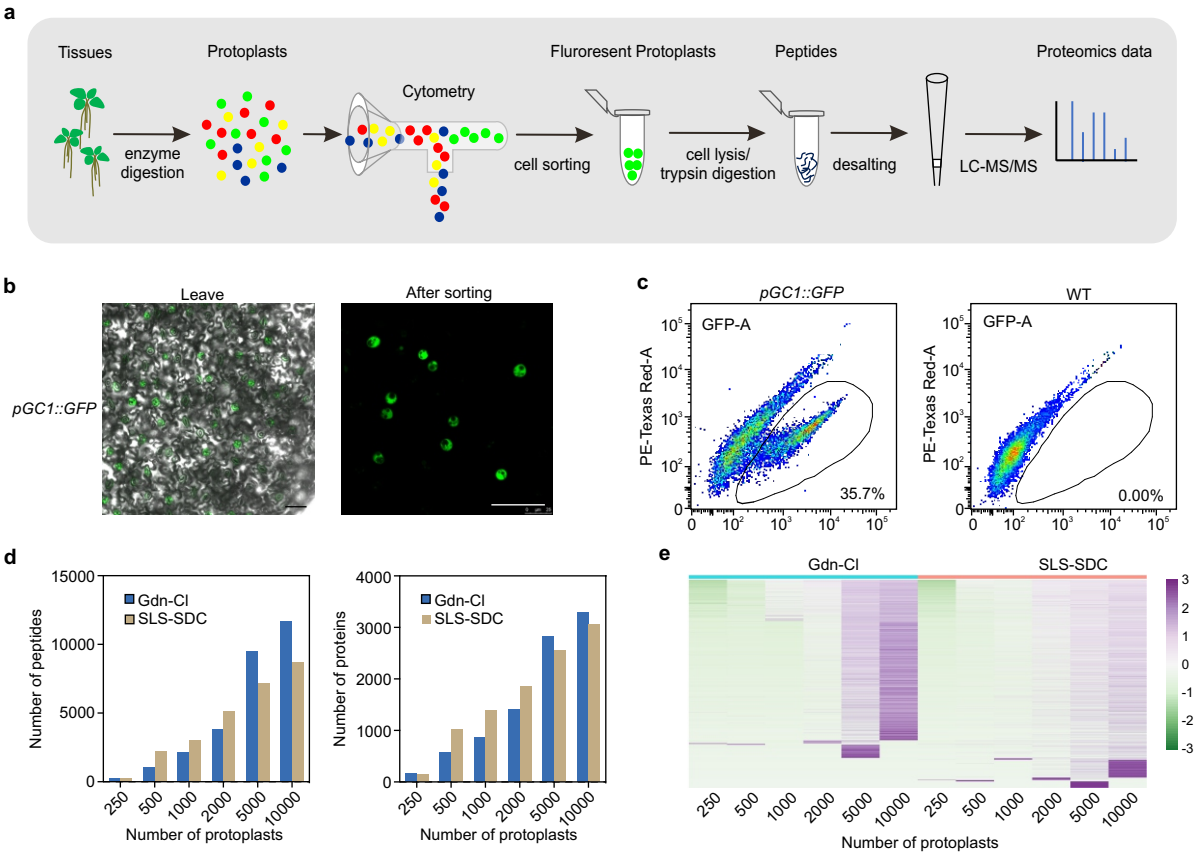
a
Tissues
Protoplasts
Cytometry
Fluroresent Protoplasts
Peptides
Proteomics data
enzyme digestion
cell sorting
cell lysis/ trypsin digestion
desalting
LC-MS/MS
b
Leave
After sorting
pGC1::GFP
c
pGC1::GFP
WT
GFP-A
PE-Texas Red-A
35.7%
0.00%
d
Gdn-Cl
SLS-SDC
Number of peptides
Number of proteins
Number of protoplasts
e
Gdn-Cl
SLS-SDC
Number of protoplasts

Fig. 1

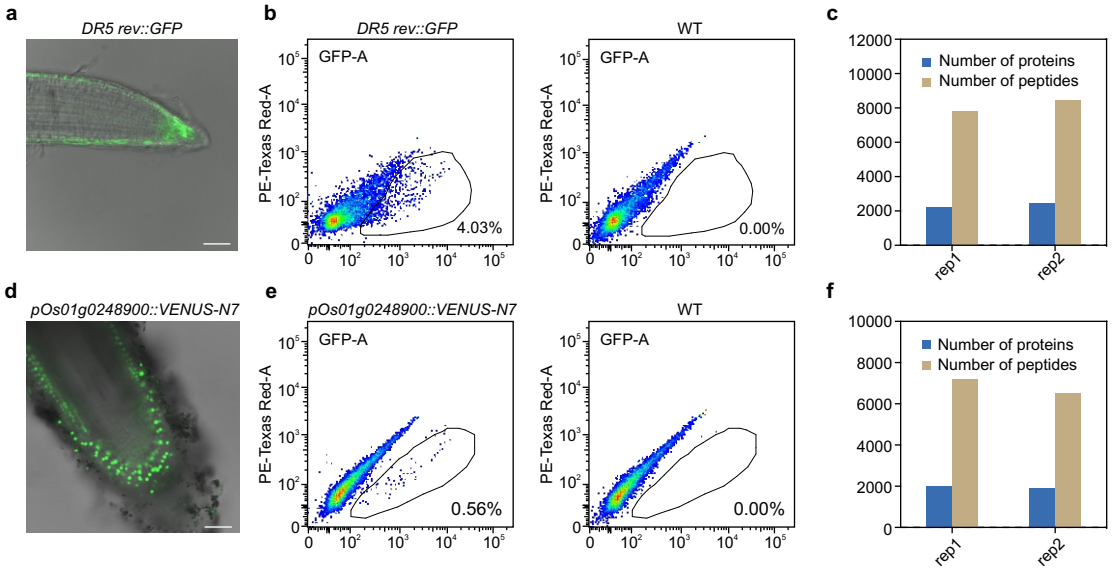
a
DR5 rev::GFP
b
DR5 rev::GFP
GFP-A
PE-Texas Red-A
4.03%
WT
GFP-A
PE-Texas Red-A
0.00%
c
Number of proteins
Number of peptides
rep1
rep2
d
pOs01g0248900::VENUS-N7
e
pOs01g0248900::VENUS-N7
GFP-A
PE-Texas Red-A
0.56%
WT
GFP-A
PE-Texas Red-A
0.00%
f
Number of proteins
Number of peptides
rep1
rep2

Fig. 2

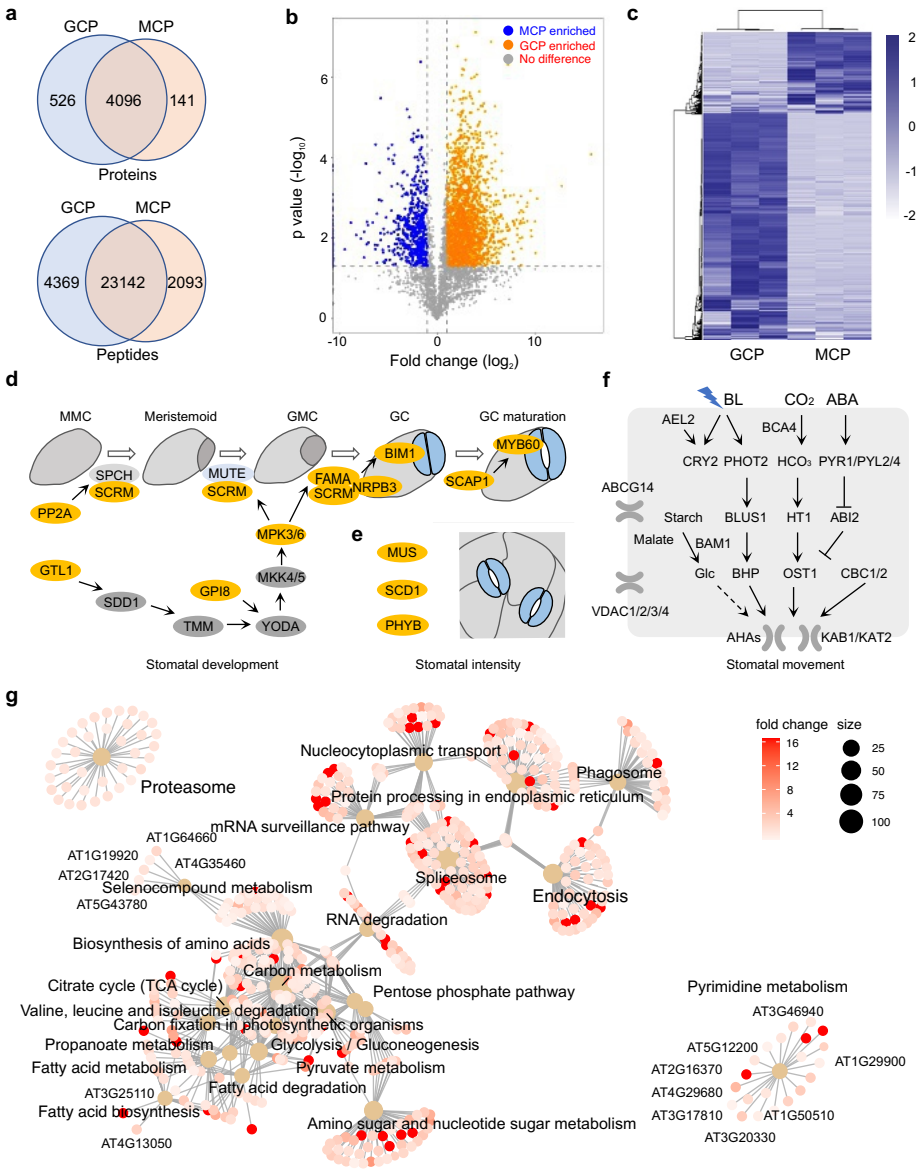
a
GCP
MCP
526
4096
141
Proteins
GCP
MCP
4369
23142
2093
Peptides
b
MCP enriched
GCP enriched
No difference
p value (-log10)
Fold change (log2)
c
GCP
MCP
d
MMC
Meristemoid
GMC
GC
GC maturation
SPCH
SCRM
PP2A
MUTE
SCRM
FAMA
SCRM
NRPB3
BIM1
SCAP1
MYB60
MPK3/6
MKK4/5
GTL1
SDD1
GPI8
TMM
YODA
Stomatal development
e
MUS
SCD1
PHYB
Stomatal intensity
f
BL
CO2
ABA
AEL2
BCA4
CRY2
PHOT2
HCO3
PYR1/PYL2/4
ABCG14
Starch
BLUS1
HT1
ABI2
Malate
BAM1
Glc
BHP
OST1
CBC1/2
VDAC1/2/3/4
AHAs
KAB1/KAT2
Stomatal movement
g
Proteasome
Nucleocytoplasmic transport
Phagosome
Protein processing in endoplasmic reticulum
mRNA surveillance pathway
AT1G64660
AT1G19920
AT4G35460
AT2G17420
Selenocompound metabolism
AT5G43780
Spliceosome
Endocytosis
RNA degradation
Biosynthesis of amino acids
Carbon metabolism
Citrate cycle (TCA cycle)
Pentose phosphate pathway
Valine, leucine and isoleucine degradation
Carbon fixation in photosynthetic organisms
Propanoate metabolism
Glycolysis / Gluconeogenesis
Fatty acid metabolism
Pyruvate metabolism
AT3G25110
Fatty acid degradation
Fatty acid biosynthesis
AT4G13050
Amino sugar and nucleotide sugar metabolism
fold change
size
Pyrimidine metabolism
AT3G46940
AT5G12200
AT1G29900
AT2G16370
AT4G29680
AT3G17810
AT1G50510
AT3G20330

Fig. 3

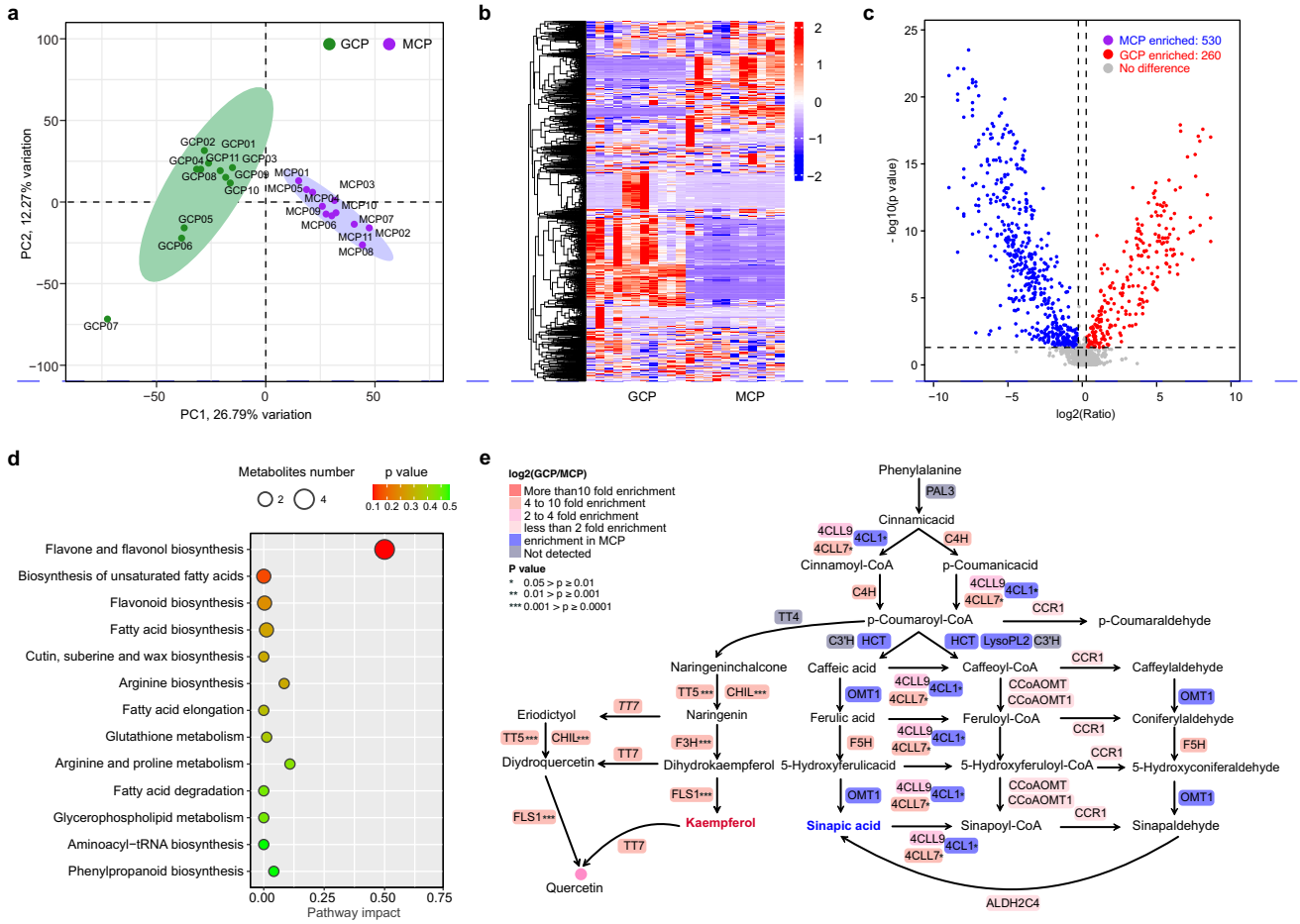
a
GCP
MCP
PC2, 12.27% variation
PC1, 26.79% variation
b
GCP
MCP
c
MCP enriched: 530
GCP enriched: 260
No difference
- log10(p value)
log2(Ratio)
d
Metabolites number
p value
Flavone and flavonol biosynthesis
Biosynthesis of unsaturated fatty acids
Flavonoid biosynthesis
Fatty acid biosynthesis
Cutin, suberine and wax biosynthesis
Arginine biosynthesis
Fatty acid elongation
Glutathione metabolism
Arginine and proline metabolism
Fatty acid degradation
Glycerophospholipid metabolism
Aminoacyl−tRNA biosynthesis
Phenylpropanoid biosynthesis
Pathway impact
e
log2(GCP/MCP)
More than10 fold enrichment
4 to 10 fold enrichment
2 to 4 fold enrichment
less than 2 fold enrichment
enrichment in MCP
Not detected
P value
Phenylalanine
PAL3
Cinnamicacid
C4H
Cinnamoyl-CoA
p-Coumanicacid
p-Coumaroyl-CoA
p-Coumaraldehyde
CCR1
Naringeninchalcone
Caffeic acid
Caffeoyl-CoA
Caffeylaldehyde
Eriodictyol
Naringenin
Ferulic acid
Feruloyl-CoA
Coniferylaldehyde
Diydroquercetin
Dihydrokaempferol
5-Hydroxyferulicacid
5-Hydroxyferuloyl-CoA
5-Hydroxyconiferaldehyde
Kaempferol
Sinapic acid
Sinapoyl-CoA
Sinapaldehyde
Quercetin
ALDH2C4

Fig. 4

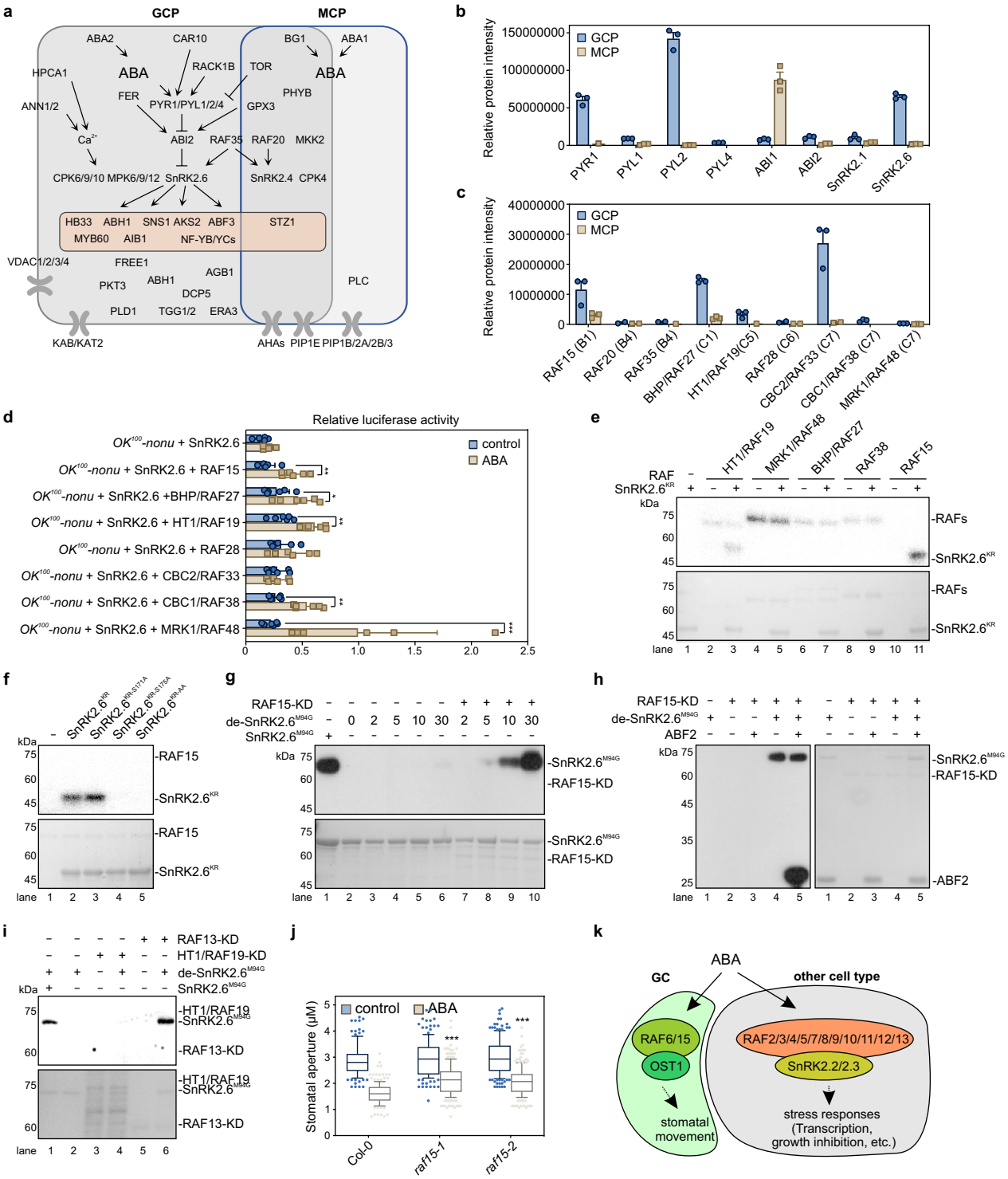
a
GCP
MCP
ABA2
CAR10
BG1
ABA1
HPCA1
ABA
RACK1B
TOR
ABA
FER
PYR1/PYL1/2/4
PHYB
ANN1/2
GPX3
Ca2+
ABI2
RAF35
RAF20
MKK2
CPK6/9/10 MPK6/9/12 SnRK2.6
SnRK2.4 CPK4
HB33 ABH1 SNS1 AKS2 ABF3
STZ1
MYB60 AIB1 NF-YB/YCs
VDAC1/2/3/4
FREE1
AGB1
ABH1
PKT3
PLC
DCP5
PLD1 TGG1/2 ERA3
KAB/KAT2
AHAs PIP1E PIP1B/2A/2B/3
b
Relative protein intensity
GCP
MCP
PYR1
PYL1
PYL2
PYL4
ABI1
ABI2
SnRK2.1
SnRK2.6
c
Relative protein intensity
GCP
MCP
RAF15 (B1)
RAF20 (B4)
RAF35 (B4)
BHP/RAF27 (C1)
HT1/RAF19(C5)
RAF28 (C6)
CBC2/RAF33 (C7)
CBC1/RAF38 (C7)
MRK1/RAF48 (C7)
d
Relative luciferase activity
control
ABA
OK100-nonu + SnRK2.6
OK100-nonu + SnRK2.6 + RAF15
OK100-nonu + SnRK2.6 +BHP/RAF27
OK100-nonu + SnRK2.6 + HT1/RAF19
OK100-nonu + SnRK2.6 + RAF28
OK100-nonu + SnRK2.6 + CBC2/RAF33
OK100-nonu + SnRK2.6 + CBC1/RAF38
OK100-nonu + SnRK2.6 + MRK1/RAF48
e
RAF
SnRK2.6KR
HT1/RAF19
MRK1/RAF48
BHP/RAF27
RAF38
RAF15
kDa
-RAFs
-SnRK2.6KR
lane
f
SnRK2.6KR
SnRK2.6KR-S171A
SnRK2.6KR-S175A
SnRK2.6KR-AA
-RAF15
-SnRK2.6KR
lane
g
RAF15-KD
de-SnRK2.6M94G
SnRK2.6M94G
-SnRK2.6M94G
-RAF15-KD
lane
h
RAF15-KD
de-SnRK2.6M94G
ABF2
-SnRK2.6M94G
-RAF15-KD
-ABF2
lane
i
RAF13-KD
HT1/RAF19-KD
de-SnRK2.6M94G
SnRK2.6M94G
-HT1/RAF19
-SnRK2.6M94G
-RAF13-KD
lane
j
Stomatal aperture (μM)
control
ABA
Col-0
raf15-1
raf15-2
k
ABA
GC
other cell type
RAF6/15
OST1
stomatal movement
RAF2/3/4/5/7/8/9/10/11/12/13
SnRK2.2/2.3
stress responses (Transcription, growth inhibition, etc.)

Fig. 5